Progress in PHOTOVOLTAICS

PROGRESS IN PHOTOVOLTAICS: RESEARCH AND APPLICATIONS
Prog. Photovolt: Res. Appl. 2017; **25**:14–22
Published online 16 October 2016 in Wiley Online Library (wileyonlinelibrary.com). DOI: 10.1002/pip.2837

ACCELERATED PUBLICATION

Cu_2ZnSnS_4 photovoltaic cell with improved efficiency fabricated by high-temperature annealing after CdS buffer-layer deposition

Shin Tajima*, Mitsutaro Umehara, Masaki Hasegawa, Takahiro Mise and Tadayoshi Itoh

Toyota Central R&D Labs., Inc., 41-1 Yokomichi, Nagakute, Aichi 480-1192, Japan

ABSTRACT

To improve the photovoltaic properties of Cu_2ZnSnS_4 (CZTS) cells, we investigated the effect of both the thickness of the deposited CdS layers and the post-annealing temperature following CdS deposition on the photovoltaic properties of CZTS cells using a two-layer CZTS structure. By depositing a thin CdS layer (40 nm) followed by high temperature annealing (603 K), we observed a remarkable increase in the short-circuit current density because of the enhancement of the external quantum efficiency in the wavelength range of 400–800 nm. The best CZTS cell exhibited a conversion efficiency of 9.4% in the active area (9.1% in the designated area). In addition, we also fabricated a CZTS cell with open-circuit voltage of 0.80 V by appropriately tuning the composition of the CZTS layers. Copyright © 2016 John Wiley & Sons, Ltd.

KEYWORDS

CZTS; CdS; post-annealing; photovoltaics; thin films

***Correspondence**

Shin Tajima, Toyota Central R&D Labs., Inc., 41-1 Yokomichi, Nagakute, Aichi 480-1192, Japan.
E-mail: e0954@mosk.tytlabs.co.jp

Received 1 December 2015; Revised 30 July 2016; Accepted 27 September 2016

1. INTRODUCTION

The compound semiconductor Cu_2ZnSnS_4 (CZTS, a Se-free system) is a promising material for photovoltaic cells [1] because none of its constituent elements are rare (e.g., In and Ga) or harmful (e.g., Se and Te), and it has a suitable band gap energy (E_g) of 1.4–1.5 eV. However, the previously reported maximum conversion efficiency (η) of CZTS cells was 8.8%, [2–8] which is significantly lower than those for $Cu(In,Ga)Se_2$ (CIGS) and CdTe cells.

To improve the open-circuit voltage (V_{oc}) of CZTS cells, we proposed a two-layer structure of CZTS absorber layers, comprising a first Cu-rich layer next to a Mo electrode and a second Cu-poor layer near the surface [7]. The difference in the Cu content between these layers formed a carrier-concentration gradient in the CZTS absorber layer, which influenced the carrier transport similarly to the effect in a p-i-n-type cell. It also increased the inner potential between the CZTS and the window layers. Using this two-layer structure, we improved the V_{oc} of the CZTS cells from 0.66 to 0.78 V and achieved $\eta = 8.8\%$.

However, the short-circuit current density (J_{sc}) in the CZTS cells was insufficiently high (17.3 mA/cm^2). Four main factors contribute to the low J_{sc} value: (i) a high positive conduction-band offset (CBO) at the interface between the buffer and CZTS layers [9,10]; (ii) increased interface recombination at the interface between the buffer and the CZTS layers [11], (iii) a low external quantum efficiency (EQE) for short-wavelength light because of absorption losses caused by the CdS buffer layer [12]; and (iv) a low EQE for long-wavelength light because of the low diffusion length of minority carriers (low mobility and/or low life time of excited electrons) [13–15]. However, X-ray photoelectron spectroscopy (XPS), pump/probe ultraviolet photoelectron spectroscopy (UPS), and UPS/inverse photoelectron spectroscopy have previously revealed [16–18] that the CBO value at the interface between the CdS and CZTS layers can lead to high-performance cells. Therefore, a high positive CBO value is not the main reason for the low J_{sc} observed in CZTS cells.

Two strategies can be envisaged to overcome the low EQE for short-wavelength light: first by using a wide-E_g (>3 eV) buffer layer, and second by having a relatively thin CdS buffer layer. Wide-E_g buffer layers such ZnS and Zn(O,S) have been reported for CZTS cells [19,20]. However, the photovoltaic properties of CZTS cells using these materials are lower than those using CdS buffer

layers. CdS has good lattice matching with CZTS and the epitaxial junction is formed at the interface between CdS and CZTS [21]; therefore, recombination at the interface should be insignificant compared with that at the interface of CZTS cells with wide-E_g buffer layers. We previously investigated the effect of the thickness of the CdS buffer layer on the photovoltaic properties of CZTS cells and found that ~100 nm was the optimal thickness because thinner CdS layers caused a high leakage current, reducing the photovoltaic properties [6]. However, we concluded that the thickness was excessive compared with that of CIGS cells [22–24]; hence, a thinner CdS layer should improve the photovoltaic properties of CZTS cells.

There are very few reports on the effect of the annealing conditions following CdS deposition in the fabrication of CZTS cells. Kijima et al. reported the effect for CIGS cells: high-temperature annealing above 573 K reduced the photovoltaic properties of the cells [23]. We previously reported that post-annealing at an appropriate temperature (~573 K) after depositing 100-nm-thick CdS layers improved the efficiency of CZTS cells [21]. In the present study, we investigated the combined effect of the thickness of CdS layers (<100 nm) and the post-annealing temperature following CdS deposition on the photovoltaic properties of CZTS cells. We find that an appropriate post-annealing temperature improved the J_{sc} of the CZTS cells when using thinner CdS layers with no increase in the leakage current, yielding a CZTS cell with $\eta = 9.4\%$.

2. EXPERIMENTAL DETAILS

The basic fabrication method for the CZTS cells is described in our previous papers [6,7,21]. First, 0.7-μm-thick Mo electrode layers were formed on alkali-glass substrates (alkali-glass: PV200, Asahi Glass Co. Ltd.) by sputter deposition. A two-layer structure was adopted for the CZTS absorber layers with a total thickness of ~1200 nm. To fabricate the first CZTS layers [CZTS(1), $t = 400$ nm], precursors were deposited by electron-beam and RF magnetron sputtering deposition using Cu, Sn, and ZnS targets to form a Cu/Sn/ZnS/Mo/alkali-glass structure, which was then sulfurized at 853 K for 20 min in 20 vol% H_2S and 80 vol% N_2 at atmospheric pressure. The heating and cooling rates were 5 and 10 K/min, respectively. The second CZTS layers [CZTS(2), $t = 800$ nm] was similarly fabricated by depositing the second set of precursors to form ZnS/Sn/Cu/CZTS (1)/Mo/alkali-glass and sulfurizing them in H_2S-N_2 gas at 773 K for 60 min. The overall compositions of the layers were measured by X-ray fluorescence (XRF) analysis. The phases in the layers were identified using X-ray diffraction (XRD) using Cu Kα X-ray source and Raman spectroscopy (excitation light: 532 nm, 0.1 mW). The CdS buffer layers were grown on the CZTS absorber layers by a chemical bath deposition (CBD) method from an aqueous solution containing Cd $(CH_3COO)_2{\cdot}2H_2O$ (3 mM), aqueous ammonia (2.5 M), and thiourea (40 mM). No etching was carried out prior to CdS deposition. The reaction solution was heated in a water bath at 358 K. The thickness of the CdS layers was controlled to be within the range of 10–100 nm by tuning the deposition time (3–12 min), and the deposition was conducted in a single run. After the deposition of Cd, the specimens were rinsed with deionized water and were annealed at 473–633 K for 20 min. In the case of a CZTS layer with a low Cu/Sn ratio (high Sn concentration), it was observed that large amounts of large size CdS colloids were often deposited on the surface of the CZTS layers for long deposition time. The formation of a thick CdS layer degraded the photovoltaic properties of the CZTS cells. However, the composition of the given CZTS layer was controlled to an appropriate value (Cu/Sn ratio: 1.8 – 2.0); therefore, the CdS colloids were barely deposited on the surface. The values for the overall compositions, thickness, and annealing temperature for the CZTS are listed in Table I. Note that the overall compositions were near-stoichiometry compared to that reported by Katagiri (Cu-poor and Zn-rich composition) [25]. A 100-nm-thick Ga-doped (5.7 wt.%) ZnO window layer (GZO) was formed by sputter deposition at room temperature. The average transmittance of the GZO layer was 89% in the range from 380 to 780 nm, and the resistivity was 4.0×10^{-4} Ωcm (mobility: 18 cm^2/Vs; carrier concentration: 5.2×10^{20} cm^{-3}) at a thickness of 400 nm. The optical E_g of the GZO layer was 3.9 eV. Finally, comb-shaped Al electrodes were formed by electron-beam deposition. The cell structure did not include an antireflection coating. The total area of the cells was approx. 0.57 cm^2, and the area of the Al electrode was 3% of the total area.

The current density–voltage (*J–V*) characteristics, η, V_{oc}, J_{sc}, and fill factor (*FF*) of the CZTS cells, were measured using a solar simulator under 1 sun and 1.5 air mass (AM) (100 mW/cm^2) illumination at 298 K (using a Peltier system isothermal plate). The parallel (R_p) and series resistances (R_s) were estimated from the *J–V* curves using the method reported by Hegedus *et al*. [26]. The microstructures of the cells were observed using a scanning transmission electron microscope coupled with energy dispersive X-ray analysis (STEM-EDX). The elemental distribution and diffusion depth of Cd into the CZTS layers were measured by three dimensional atom-probe tomography (3D APT) [7,21].

3. RESULTS AND DISCUSSION

The phases and microstructure of the CZTS layers are shown in Figures 1, 2, and 3. No impurity phases are observed by the XRD profiles of one- or two-layered CZTS (Figure 1). The Raman spectroscopy confirms that the layer was CZTS, as shown in Figure 2 [27]. However, both the Raman peaks at 287 and 373 cm^{-1} are weak, suggesting that the CZTS has some structure disorder (e.g., Cu and Zn cation disorder), as has been reported previously [28,29]. In Figure 3, it is seen that a MoS_X layer is

Table I. Types and compositions of the CZTS layers, CdS thicknesses, and annealing temperatures following CdS deposition.

No.	Type	Cu/(Zn + Sn)	Zn/Sn	CdS thickness (nm)	Annealing (K)
ref. 1[6]	One-layer	0.88	1.20	100	543
ref. 2[7]	Two-layer	0.94	1.07	100	543
1	One-layer	0.88	1.20	40	543
2	One-layer	0.88	1.20	40	603
3	Two-layer	0.94	1.07	10	603
4	Two-layer	0.94	1.07	20	603
5	Two-layer	0.94	1.07	40	none
6	Two-layer	0.94	1.07	40	473
7	Two-layer	0.94	1.07	40	543
8	Two-layer	0.94	1.07	40	573
9	Two-layer	0.94	1.07	40	603
10	Two-layer	0.94	1.07	40	633
11	Two-layer	0.94	1.07	60	603
12	Two-layer	0.94	1.07	80	603
13	Two-layer	0.90	1.07	40	603

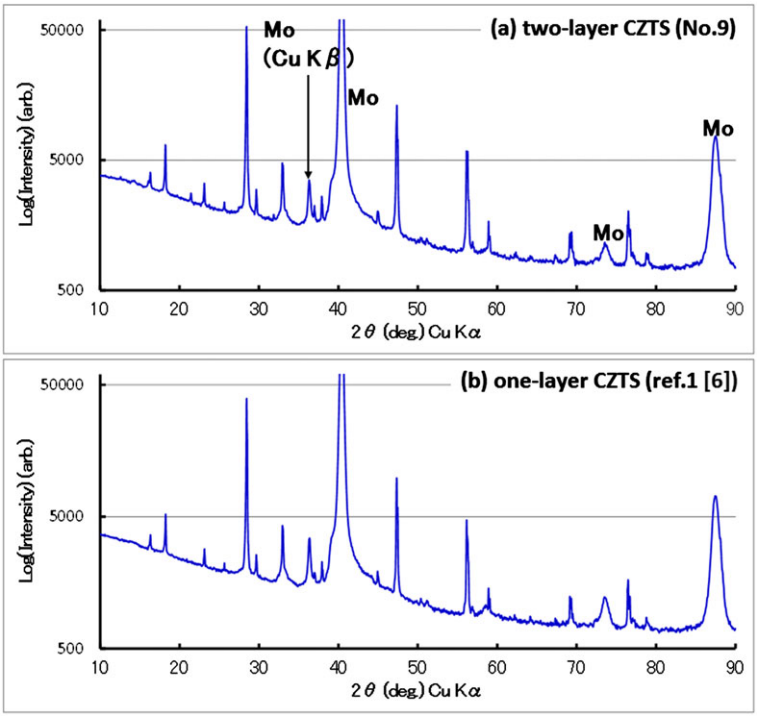

Figure 1. X-ray diffraction profiles of the one-layer and two-layer structured CZTS. The peaks without a marker are identified to be CZTS (PDF#00-026-0575).

formed at the interface of CZTS/Mo and ZnS in the CZTS layer as conformed by STEM-EDX, and that the CZTS layer has a porous structure [7]. The presence of phase disorder, the microstructure, and the MoS_X layer could lead to high R_s and low mobility, and decrease the photovoltaic performance [30–32].

Tables II and III summarize the photovoltaic properties of the CZTS cells examined in this study (Table II: effect of the annealing temperature following CdS deposition and Table III: effect of the thickness of CdS layers). The *J–V* curves and EQE spectra of ref. 2, cell Nos. 1 and 9 are shown in Figures 4 and 5 as relevant examples for the following reasons:

Ref. 2 cell The highest efficiency reported in a previous work (two-layered CZTS with thick CdS and low temperature annealing)

Cell No. 1 Low efficiency (thin CdS buffer layer, but one-layered CZTS, and low temperature annealing)

Cell No. 9 The highest efficiency among the cells tested in this work (two-layered CZTS, thin CdS buffer layer, and high temperature annealing)

DOI: 10.1002/pip

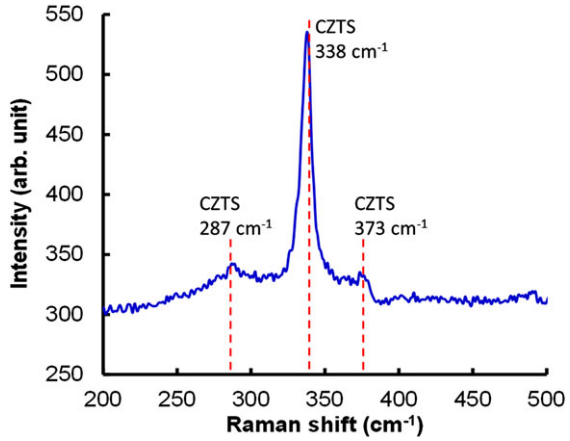

Figure 2. Raman spectroscopy of two-layer CZTS (excitation light: 532 nm, 0.1 mW). Three peaks were identified as CZTS [20].

The influence of the CdS thickness and the annealing temperature can be determined from these *J–V* curves. For the one-layer-structured CZTS cells post-annealed at 543 K (ref. 1 and No. 1), R_p decreased with CdS layer thickness. However, when the annealing temperature was increased from 543 to 603 K (No. 2), the *FF* improved to the same value that was obtained using a 100-nm-thick CdS layer. This result indicates that annealing after the CdS layer deposition improves the photovoltaic properties of CZTS cells.

Table II. Relationship between the annealing temperature after CdS deposition and the photovoltaic properties of the CZTS cells under 1 sun and 1.5 AM (100 mW/cm^2) illumination at 298 K. [thickness of the CdS layer: 100 nm (ref. 1 and 2) or 40 nm (1, 2, 5–10, 13)]

No.	Annealing (K)	η(%)	J_{sc} (mA/cm^2)	V_{oc} (V)	*FF*	R_p (Ωcm^2)	R_s (Ωcm^2)
ref. 1[6]	543	7.6	20.1	0.66	0.57	450	0.8
ref. 2[7]	543	8.8	17.5	0.71	0.71	1700	1.0
1	543	5.3	19.4	0.63	0.43	190	3.0
2	603	8.7	21.5	0.71	0.57	430	2.5
5	none	5.0	16.0	0.72	0.43	650	3.7
6	473	6.0	16.3	0.72	0.51	600	2.5
7	543	7.0	16.2	0.72	0.60	650	1.5
8	573	7.9	18.4	0.72	0.60	580	1.3
9	603	9.4	21.3	0.70	0.63	620	1.2
10	633	5.3	19.9	0.65	0.41	170	3.5
13	603	8.7	18.1	0.80	0.60	900	2.1

Therefore, we investigated both the effect of the CdS layer thickness and that of the annealing temperature following CdS deposition, in the case of two-layered CZTS. First, we investigated the relationship between the photovoltaic properties and the CdS layer thickness at the annealing temperature of 603 K (Nos. 3, 4, 9, 11, and 12). When the thickness increased from 10 to 40 nm, both η

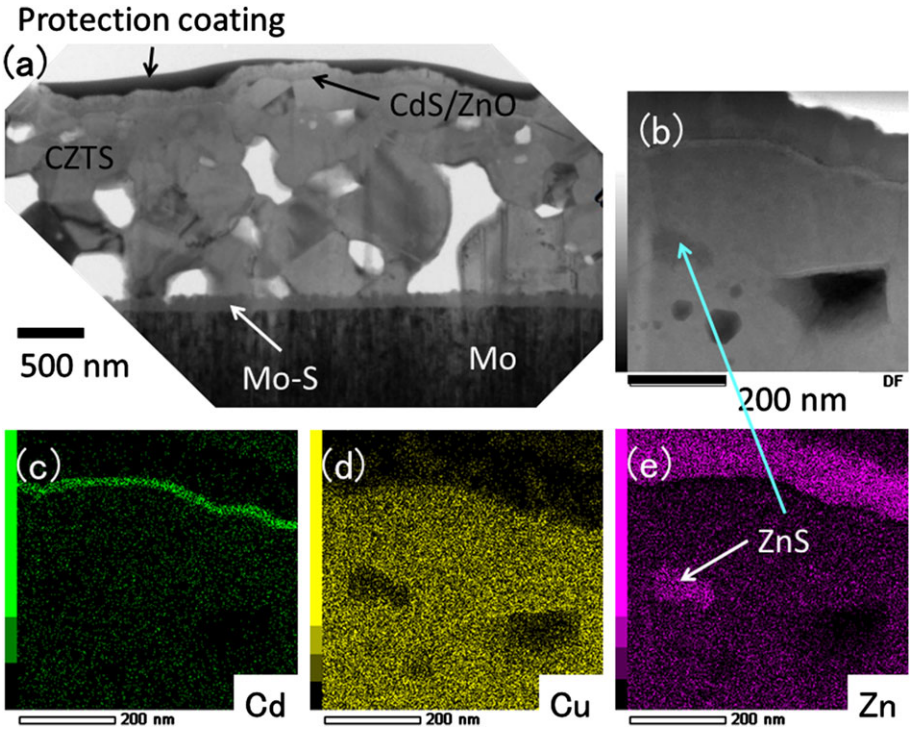

Figure 3. (a) Bright-field TEM photograph of the cross section of CZTS cells. (b) Dark-field TEM photograph and (c)–(e) EDX of the cross-section of the CZTS cells; (b)–(e) were observed in the same region. ZnS grains are observed in (e).

Table III. Relationship between the thicknesses of CdS layers and photovoltaic properties of the CZTS cells under 1 sun and 1.5 AM (100 mW/cm^2) illumination at 298 K. (annealing temperature following CdS deposition: 603 K)

No.	CdS thickness (nm)	η(%)	J_{sc} (mA/cm^2)	V_{oc} (V)	FF	R_p (Ωcm^2)	R_s (Ωcm^2)
3	10	2.6	14.2	0.65	0.28	90	9
4	20	6.2	17.7	0.73	0.48	520	3.5
9	40	9.4	21.3	0.70	0.63	620	1.2
11	60	8.1	18.0	0.76	0.59	830	2.0
12	80	8.1	18.1	0.75	0.60	840	1.5
13	40	8.7	18.1	0.80	0.60	900	2.1

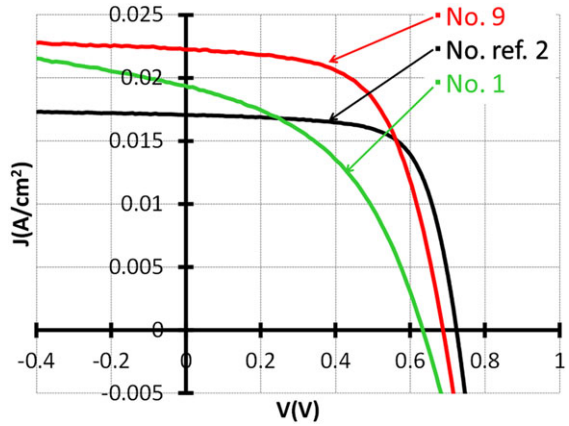

Figure 4. *J–V* curves of CZTS cells (Nos. ref. 2 [7], 1, and 9) under 1 sun and 1.5 AM (100 mW/cm^2) illumination at 298 K.

and J_{sc} improved and the maximum values were obtained for 40 nm. However, a further increase in the thickness degraded the performance. In case of thinner CdS layers, the leakage current increased because of the fact that the CdS layers did not entirely cover the CZTS layers. On the other hand, for thicker CdS layers, the absorption loss by the CdS layers in the short-wavelength range was increased, decreasing the J_{sc}. Therefore, 40 nm was the optimal thickness of the CdS layers for annealing at 603 K. Next, the effect of the annealing temperature after the CdS layer deposition on the photovoltaic properties was investigated (Nos. 5, 6, 7, 8, 9, and 10). The J_{sc} (and consequently η) improved remarkably as the annealing temperature increased from 473 to 603 K. However, higher temperatures, namely 633 K, caused a rapid decrease in the FF and R_p.

By optimizing both the CdS layer thickness and the post-annealing temperature, the best performance was achieved for sample No. 9 with η as high as 9.4%. In order to verify this result, the photovoltaic properties of sample No. 9 was precisely measured at the National Institute of Advanced Industrial Science and Technology (AIST) in Japan [33]. In addition, the EQE spectra of sample No. 9 show significantly improved values for not only short-wavelength light (300–550 nm) but also long-wavelength light (600–800 nm), as shown in Figure 5, yielding a high J_{sc} of 21.3 mA/cm^{-2}. Note that the average reflection loss for the CZTS cells from 400 to 800 nm was estimated to be approximately 10% using a spectrophotometer. The enhancement in the short-wavelength range was because of the decrease in the absorption loss of the CdS layer; however, the reason for the improvement in the long-wavelength range is unknown. In order to further investigate this, the elemental distribution at the CdS/CZTS interface was investigated. The diffusion depth of Cd into CZTS cells (No. 9) was measured by 3D APT, and the results are shown in Figure 6. It is seen that the Cd concentration is approximately 5 at.% in the CZTS layers near the CdS/CZTS interface. STEM-EDX measurements have estimated the total Cd concentration over all the CZTS layers as shown in Figure 3. These measurements have confirmed that Cd is not detected in CZTS layers at distance > 100 nm from the interface of CdS/CZTS. We have previously reported the effect of the post-annealing temperature on the photovoltaic performances for cells

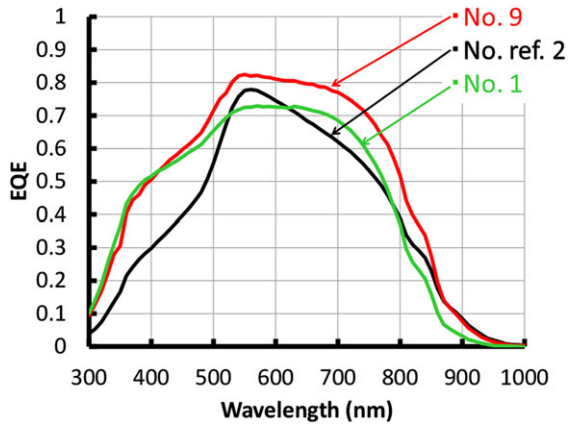

Figure 5. EQE spectra of CZTS cells (Nos. ref. 2 [7], 1, and 9) at 0 V bias and at 298 K.

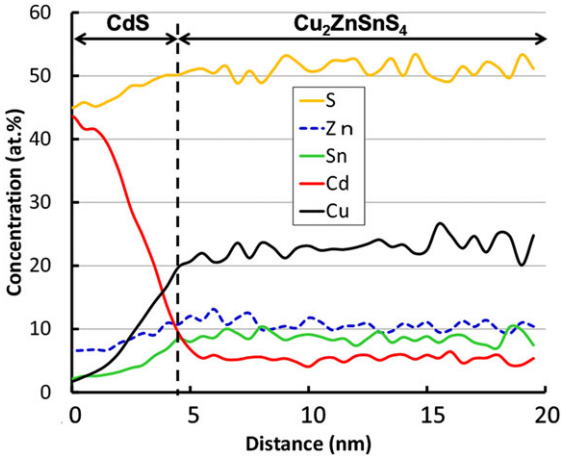

Figure 6. Elemental distribution obtained using 3D APT at the CdS/CZTS interface in the CZTS cell (No. 11) annealed at 603 K after CdS deposition.

DOI: 10.1002/pip

where 100-nm-thick CdS layers were used [21]. It was observed that Cd atoms diffused from the CdS layers into the CZTS layers, and $Cu_2(Zn,Cd)SnS_4$ was formed on the surface of the CZTS layers. We investigated the properties of Cd-doped CZTS sintered bodies using previous literature [30]. The Cd-doped CZTS sintered bodies had a high mobility (several cm^2/Vs), a low hole carrier concentration (below $10^{15}\,cm^{-3}$), and a low Seebeck coefficient of approximately +10 μV/K, which means that the semiconductor properties changed from *p*-type to intrinsic. (This study could not be done on Cd-doped CZTS layers because it is very difficult to characterize semiconductor layers on Mo-coated glass.) In addition, the thermal conductivity of the Cd-doped CZTS sintered bodies at 20 K was higher when compared to that of CZTS, which indicated that the number of defects, which caused phonon scattering in the CZTS, was reduced in the Cd doped samples [30]. This result implies that Cd diffusion could cause band bending and an increase in the mobility of the excited electron in the vicinity of the surface of the CZTS layer, resulting in the increase of J_{sc} [21]. On the other hand, annealing at 633 K caused the segregation of ZnS at the CdS/CZTS interface that degraded the photovoltaic properties. From previous research [21] and based on our experimental results, a schematic of the CZTS cell structure formed after annealing at 603 K following the deposition of a thin CdS layer was constructed, as shown in Figure 7. The thickness of the Cd-doped CZTS layer was estimated by 3D-APT [21].

In addition, both Cd diffusion into CZTS layers and Zn diffusion into CdS can change the CBO at the interface of CdS/CZTS [21,34]. The spike-type CBO is advantageous to optimize the properties of the CZTS cells [9,10]. The CBO could become spike-type when (Cd,Zn)S solid solution was formed because of the Zn diffusion into CdS in view of the fact that the CBM of (Cd,Zn)S shifted to a more positive level [34]. Indeed, Terada et al. indicated that the CdS/CZTS interface changed to a spike-type (positive) CBO because of annealing following CdS deposition [18]. In contrast, in the case of the cells annealed at low temperature or no anneal after CdS deposition, the CdS/CZTS interfaces possess a flat or cliff-type CBO [16,17,35]. However, the CBO at the interface of CdS/CZTS annealed at high temperature must be investigated in detail in order to discuss its influence on the properties of CZTS cells.

As described above, this result implies that the Cd diffusion into the CZTS and the Zn diffusion into CdS improve the characteristics of the CZTS layer and the interface of CdS/CZTS (a decrease in defect concentration, increase in the mobility, the positive CBO, etc.), thereby increasing the EQE in the long-wavelength range. Furthermore, the CZTS cell exhibited a high J_{sc} (>21 mA/cm^{-2}) and a high η (>9%). We therefore conclude that the post-annealing following CdS deposition was effective in improving the photovoltaic properties of the CZTS cells.

The influence of the composition of the CZTS absorber layers was also investigated (Nos. 9 and 13). Sample No.13, in which the CZTS layer had a Cu-poor composition compared with sample No. 9, had a higher V_{oc} of 0.80 V, whereas its J_{sc} was smaller compared to No. 9 (Figure 8). In the case of thin, high-performance, compound-semiconductor, photovoltaic cells, the target V_{oc} should be higher than the value that is usually calculated using the equation $V_{oc} = (E_g/e) - 0.5$ (CZTS cells: > 0.9 V) [24]. Note that the equation gives an empirical estimate for practical purposes and does not imply a theoretical maximum. The increase in the V_{oc} of sample No. 13 may have been caused by the large difference in the Cu

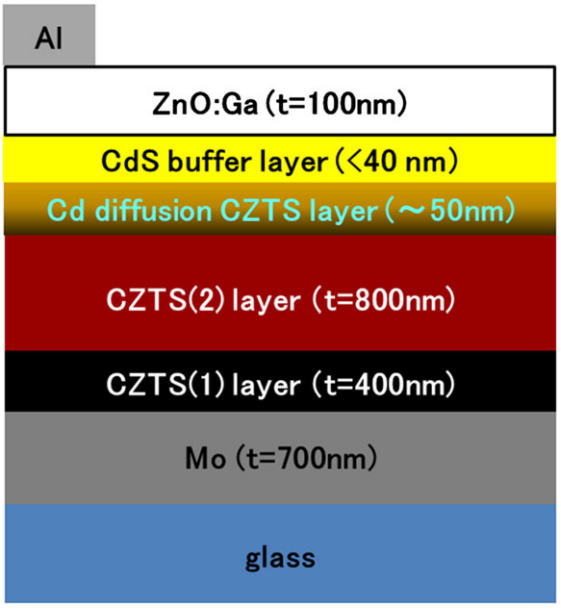

Figure 7. Schematic of the CZTS cell after high-temperature annealing (603 K) following the deposition of a thin CdS layer ($t < 40$ nm). The thickness of the Cd-doped CZTS layer was estimated by 3D-APT [21].

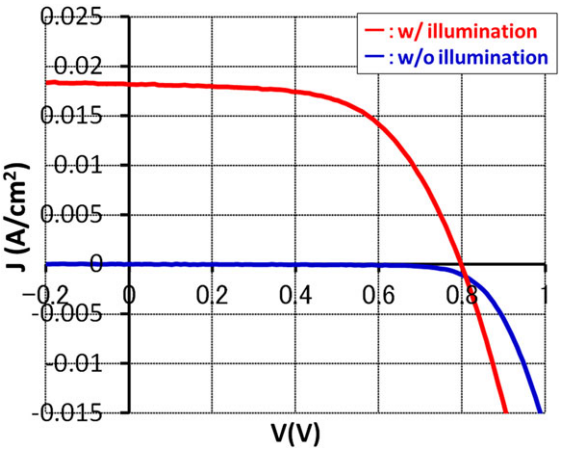

Figure 8. *J–V* curves of the CZTS cell (No. 13) with a high V_{oc} of 0.80 V under 1 sun and 1.5 AM (100 mW/cm^2) illumination at 298 K. A crossover behavior between the curves with and without illumination is clearly observed.

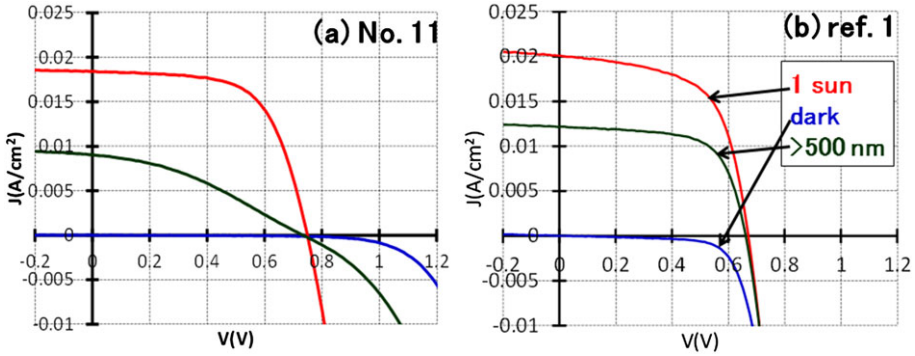

Figure 9. Dependence of the *J–V* curves of CZTS cells on the wavelength of illumination at 298 K. (1 sun: 1 sun and 1.5 AM (100 mW/cm^2) illumination, > 500 nm: The illumination was that of 1 sun and 1.5 AM limited to above 500 nm using a long-wavelength pass filter).

content between the CZTS(1) and CZTS(2) layers induced by the low Cu content of CZTS(2) and the overall Cu-poor composition because the overall chemical composition of CZTS(1) was kept constant. Simultaneously, the low Cu content of the CZTS(2) layer reduced the carrier concentration of this layer, resulting in high *Rs* and low J_{sc}.

In **Figure** 8, a crossover behavior, i.e., the crossover of the dark and illuminated *J–V* curves near $J = 0$, is observed in the *J–V* curves while R_s under dark conditions increased when compared to that under illumination. The CZTS cells using thin CdS layers with thicknesses < 60 nm and high-temperature (>573 K) post-annealing (Nos. 2, 4, 8, 9, 11, 13) had similar crossover behaviors in the *J–V* curves. The crossover was also observed after the cells were light-soaked for 10 min under open-circuit conditions at room temperature. In contrast, cells with thick CdS layers and/or those obtained using low-temperature post-annealing (e.g., Nos. ref. 1, ref. 2, 1, and 5–7) did not exhibit crossover behavior. (The CdS layer in No. 3 was too thin to act as an effective buffer layer, and cell No. 10 was overheated.) To investigate the reason for the crossover, the dependence of the *J–V* curves of the CZTS cells on the illumination wavelengths was investigated using a sharp-cutoff long-wavelength-pass filter with a cutoff wavelength of 500 nm, as shown in Figure 9. In the case of ref. 1, the crossover is not observed regardless of the wavelength of illumination. On the other hand, at long wavelengths (>500 nm), 'red-kink' is also observed concurrently with the crossover in the case of No. 11, while R_s under dark conditions increases significantly compared to that under illumination. The wavelength of 500 nm, which corresponds to a photon energy of 2.5 eV, agrees with the measured E_g of the CBD–CdS layer.

Generally, it was considered that the occurrence of crossover and red-kink reduced the performance of photovoltaic cells [24,36,37]. However, in this work, the high performance cells also showed the crossover and/or the red-kink. In cells based on the chalcogenide system, crossover and red-kink potentially occur when the CBO at the interface of the buffer layer/the absorption layer is 'spike-type'. As described above, the CBO at the interface of the CdS/CZTS could be influenced by annealing conditions. The correlation between the annealing conditions and the occurrence of crossover and red-kink indicates that the CBO changed from a flat or cliff-type to a spike-type because of annealing at high temperature following CdS deposition. The change in the nature of the CBO could improve the properties of the CZTS cells, even while the crossover and red-kink occurred.

The crossover is generally caused by the photoactive defects, which could become acceptor-type recombination centers in the buffer layers (CdS layer in this case) [24,36–42]. A possible explanation for the red-kink could be the presence of a barrier for the photo current at the buffer layer [36,39,41,43]. Incidentally, MoS_X layers and defects at the CZTS/Mo interface could also influence the photovoltaic properties of CZTS cells. However, in this work, the effects of the MoSx layer and the defects are neglected for a comparative study of the CZTS cells because all the CZTS layers were sulfurized under the same conditions and had the same MoS_X layers and defect concentrations at the CZTS/Mo interface. Neuschitzer and Umehara reported the mechanism of the crossover and the red-kink in the CdS/CZTSe and CdS/Cu_2SnS_3 systems, respectively [37,41]. They showed that the photoactive defects in the CdS layers, such as interstitial sulfur [38], caused the crossover and the red-kink. It is possible that a similar mechanism is operative in our case. In this work, the high temperature annealing following CdS deposition could form photoactive defects at the CdS buffer layers causing crossover and red-kink to occur. If a spike type CBO at the interface of CdS/CZTS and a decrease in the defects at the CdS layer (elimination of crossover and red-kink) are simultaneously achieved, the photovoltaic properties of CZTS cells can be further improved.

4. CONCLUSIONS

We investigated the effects of the thickness of the CdS buffer layer and the annealing conditions following CdS layer deposition on the photovoltaic properties of CZTS

DOI: 10.1002/pip

cells. When CZTS cells with 40-nm-thick CdS layers were post-annealed at 603 K, the J_{sc} improved significantly. The best-performing cell exhibited $\eta = 9.4\%$, $V_{oc} = 0.70$ V, $J_{sc} = 21.3$ mA/cm^2, and $FF = 0.63$ in the active area ($\eta = 9.14\%$ in the designated area) [8]. We also fabricated a CZTS cell with $V_{oc} = 0.80$ V. Our results show that using two-layered CZTS, a thinner CdS buffer layer, and annealing at high temperature following CdS deposition were effective for the fabrication of high performance CZTS cells. In particular, Cd diffusion from CdS into CZTS and Zn diffusion from CZTS into CdS during the annealing could change the CBO at the CdS/CZTS interface from a cliff-type to a spike-type, which potentially improved the photovoltaic properties of the CZTS cells. On the other hand, annealing could also form defects at the CdS layer, resulting in the occurrence of crossover and red-kink in the *J–V* curves in CZTS cells.

ACKNOWLEDGEMENTS

We thank Dr. Y. Hishikawa of AIST for the precise measurements of the *J–V* characteristics. We also acknowledge Mr. Y. Kato for Raman spectroscopy measurement, Dr. K Ohishi for the TEM and 3D APT observations, and Mr Y. Yamashita for the device analysis.

REFERENCES

1. Ito K, Nakazawa T. Electrical and optical properties of stannite-type quaternary semiconductor thin films. *Japanese Journal of Applied Physics* 1988; **27**(11): 2094–2097.
2. Wang W, Winkler MT, Gunawan O, Gokmen T, Todorov TK, Zhu Y, Mitzi DB. Device characteristics of CZTSSe thin-film solar cells with 12.6% efficiency. *Advanced Energy Materials* 2014; **4**(7): 1301465.
3. Katagiri H, Jimbo K, Yamada S, Kamimura T, Maw WS, Fukano T, Ito T, Motohiro T. Enhanced conversion efficiencies of CZTS-based thin film solar cells. *Applied Physics Express* 2008; **1**: 041201.
4. Shin B, Zhu Y, Gershon T, Bojarczuk NA, Guha S. Epitaxial growth of kesterite Cu2ZnSnS4 on a Si (001) substrate by thermal co-evaporation. *Thin Solid Films* 2014; **556**: 9–12.
5. H. Sugimoto, C. Liao, H. Hiroi, N. Sakai, and T. Kato. Proc. PVSC 39 2013; ; MePVSC517-0615082512, July.
6. Fukano T, Tajima S, Ito T. Enhancement of conversion efficiency of Cu_2ZnSnS_4 thin film solar cells by improvement of sulfurization conditions. *Applied Physics Express* 2013; **6**(6): 062301.
7. Tajima S, Itoh T, Hazama H, Ohishi K, Asahi R. Improvement of the open-circuit voltage of Cu_2ZnSnS_4 solar cells using a two-layer structure. *Applied Physics Express* 2015; **8**(8): 082302.
8. Green MA, Emery K, Hishikawa Y, Warta W, Dunlop ED. Solar cell efficiency tables (version 46). *Progress in Photovoltaics: Research and Applications* 2015; **23**(7): 805–812.
9. Minemoto T, Matsui T, Takakura H, Hamakawa Y, Negami T, Hashimoto Y, Uenoyama T, Kitagawa M. Theoretical analysis of the effect of conduction band ofset of window/CIS layers on performance of CIS solar cells using device simulation. *Solar Energy Materials and Solar Cells* 2001; **67**: 83–88.
10. Minemoto T, Hashimoto Y, Satoh T, Negami T, Takakura H, Hamakawa Y. $Cu(In,Ga)Se_2$ solar cells with controlled conduction band offset of window/$Cu(In,Ga)Se_2$ layers. *Journal of Applied Physics* 2001; **89**(12): 8327.
11. Tajima S, Katagiri H, Jimbo K, Sugimoto N, Fukano T. Temperature dependence of Cu_2ZnSnS_4 photovoltaic cell properties. *Applied Physics Express* 2012; **5**(8): 082302.
12. Lee S, Lee ES, Kim TY, Cho JS, Eo YJ, Yun JH, Cho A. Effect of annealing treatment on CdS/CIGS thin film solar cells depending on different CdS deposition temperatures. *Solar Energy Materials & Solar Cells* 2015; **141**: 299–308.
13. H. Sugimoto, C. Liao, H. Hiroi, N. Sakai, and T. Kato. Lifetime improvement for high efficiency Cu_2ZnSnS_4 submodules, 2013IEEEPVSC723_130610100652 2013.
14. Gershon T, Shin B, Bojarczuk N, Hopstaken M, Mitzi DB, Guha S. The role of sodium as a surfactant and suppressor of non-radiative recombination at internal surfaces in Cu2ZnSnS4. *Advanced Energy Materials* 2015; **5**(2): n/a–n/a.
15. Gershon T, Shin B, Bojarczuk N, Gokmen T, Lu S, Guha S. Photoluminescence characterization of a high-efficiency Cu2ZnSnS4 device. *Journal of Applied Physics* 2013; **114**(15): 154905.
16. Tajima S, Kataoka K, Takahashi N, Kimoto Y, Fukano T, Hasegawa M, Hazama H. Direct measurement of band offset at the interface between CdS and Cu_2ZnSnS_4 using hard X-ray photoelectron spectroscopy. *Applied Physics Letters* 2013; **103**(24): 243906.
17. Haight R, Barkhouse A, Gunawan O, Shin B, Copel M, Hopstaken M, Mitzi DB. Band alignment at the $Cu_2ZnSn(S_xSe_{1-x})_4$/CdS interface. *Applied Physics Letters* 2011; **98**(25): 253502.
18. N. Terada, H. Morita, H. Chochi, S. Yoshimoto, T. Fukano, S. Tajima, K. Higuchi, H. Tampo, H. Shibata, K. Matsubara, and S. Niki, 2013 MRS Spring Meeting, C5.06.

19. Kim J, Park C, Pawar SM, Inamdar AI, Jo Y, Han J, Hong J, Park YS, Kim DY, Jung W, Kim H, Im H. Optimization of sputtered ZnS buffer for Cu2ZnSnS4 thin film solar cells. *Thin Solid Films* 2014; **566**: 88–92.
20. Ericson T, Scragg JJ, Kubart T, Törndahl T, Platzer-Björkman C. Annealing behavior of reactively sputtered precursor films for Cu2ZnSnS4 solar cells. *Thin Solid Films* 2013; **535**: 22–26.
21. Tajima S, Asahi R, Isheim D, Seidman DN, Itoh T, Hasegawa M, Ohishi K. Atom-probe tomographic study of interfaces of Cu_2ZnSnS_4 photovoltaic cells. *Applied Physics Letters* 2014; **105**: 093901.
22. Reinhard P, Chirila A, Bloesch P, Pianezzi F, Nishiwaki S, Buecheler S, Tiwari A. Review of progress toward 20% efficiency flexible CIGS solar cells and manufacturing issues of solar modules. *IEEE Photovoltaics* 2013; **3**: 572–580.
23. Kijima S, Nakada T. High-temperature degradation mechanism of Cu(in,Ga)Se_2-based thin film solar cells. *Applied Physics Express* 2008; **1**: 075002.
24. Scheer R, Schock H. *Chalcogenide Photovoltaics: Physics, Technologies, and Thin film Devices*. Wiley-VCH: Weinheim, Germany, 2011.
25. Katagiri H. CZTS thin film solar cells. *Thin Solid Films* 2005; **480–481**: 426.
26. Hegedus SS, Shafarman WN. Thin-film solar cells: device measurements and analysis. *Progress in Photovoltaics: Research and Applications* 2004; **12**(23): 155–176.
27. Nagaoka A, Yoshino K, Taniguchi H, Taniyama T, Miyake H. Preparation of Cu2ZnSnS4 single crystals from Sn solutions. *Journal of Crystal Growth* 2012; **341**(1): 38–41.
28. Valakh MY, Kolomys OF, Ponomaryov SS, Yukhymchuk VO, Babichuk IS, Izquierdo-Roca V, Saucedo E, Perez-Rodriguez A, Morante JR, Schorr S, Bodnar IV. Raman scattering and disorder effect in Cu2ZnSnS4. *Physica status solidi (RRL)—Rapid Research Letters* 2013; **7**(4): 258–261.
29. Scragg JJS, Choubrac L, Lafond A, Ericson T, Platzer-Björkman C. A low-temperature order-disorder transition in Cu2ZnSnS4 thin films. *Applied Physics Letters* 2014; **104**(4): 041911.
30. Hazama H, Tajima S, Masuoka Y, Asahi R. Transport properties of the Cu_2ZnSnS_4 bulk systems: effects of nonstoichiometry and defect formation. *Journal of Alloys and Compounds* 2016; **657**: 179–183.
31. Liu X, Cui H, Kong C, Hao X, Huang Y, Liu F, Song N, Conibeer G, Green M. Rapid thermal annealed Molybdenum back contact for Cu2ZnSnS4 thin film solar cells. *Applied Physics Letters* 2015; **106**(13): 131110.
32. Liu F, Sun K, Li W, Yan C, Cui H, Jiang L, Hao X, Green MA. Enhancing the Cu2ZnSnS4 solar cell efficiency by back contact modification: inserting a thin TiB2 intermediate layer at Cu2ZnSnS4/Mo interface. *Applied Physics Letters* 2014; **104**(5): 051105.
33. Green MA, Emery K, Hishikawa Y, Warta W, Dunlop ED. Solar cell efficiency tables (version 42). *Progress in Photovoltaics: Research and Applications* 2013; **21**(5): 827–837.
34. Wu J-C, Zheng J, Zacherl CL, Wu P, Liu Z-K, Xu R. Hybrid functionals study of band bowing, band edges and electronic structures of Cd1–xZnxS solid solution. *The Journal of Physical Chemistry C* 2011; **115**(40): 19741–19748.
35. Terada N, Yoshimoto S, Chochi K, Fukuyama T, Mitsunaga M, Tampo H, Shibata H, Matsubara K, Niki S, Sakai N, Katou T, Sugimoto H. Characterization of electronic structure of $Cu_2ZnSn(S_xSe_{1-x})_4$ absorber layer and $CdS/Cu_2ZnSn(S_xSe_{1-x})_4$ interfaces by in-situ photoemission and inverse photoemission spectroscopies. *Thin Solid Films* 2015; **582**: 166–170.
36. Pudov AO, Sites JR, Contreras MA, Nakada T, Schock HW. CIGS J–V distortion in the absence of blue photons. *Thin Solid Films* 2005; **480–481**: 273–278.
37. Neuschitzer M, Sanchez Y, López-Marino S, Xie H, Fairbrother A, Placidi M, Haass S, Izquierdo-Roca V, Perez-Rodriguez A, Saucedo E. Optimization of CdS buffer layer for high-performance Cu2ZnSnSe4solar cells and the effects of light soaking: elimination of crossover and red kink. *Progress in Photovoltaics: Research and Applications* 2015; **23**(11): 1660–1667.
38. Nishidate K, Sato T, Matsukura Y, Baba M, Hasegawa M, Sasaki T. Density-functional electronic structure calculations for native defects and Cu impurities in CdS. *Physical Review B* 2006; **74**(3): 035210.
39. Eisgruber IL, Granata JE, Sites JR, Hou J, Kessler J. Blue-photon modiÞcation of nonstandard diodebarrier in CuInSe2 solar cells. *Solar Energy Materials & Solar Cells* 1998; **53**: 367–377.
40. Wang K, Gunawan O, Todorov T, Shin B, Chey SJ, Bojarczuk NA, Mitzi D, Guha S. Thermally evaporated Cu2ZnSnS4 solar cells. *Applied Physics Letters* 2010; **97**(14): 143508.
41. Umehara M, Takeda Y, Tajima S, Motohiro T, Sakai T, Maekawa R. Improvement of red light response of Cu2Sn1 − xGexS3 solar cells by optimization of CdS buffer layers. *Journal of Applied Physics* 2015; **118** (15): 154502.
42. Nagoya A, Asahi R, Wahl R, Kresse G. Defect formation and phase stability ofCu_2ZnSnS_4 photovoltaic material. *Physical Review B* 2010; **81**(11): 113202.
43. Kylner A. Effect of impurities in the CdS buffer layer on the performance of the Cu(In,Ga)Se2 thin film solar cell. *Journal of Applied Physics* 1999; **85**: 6858–6865.